



# Effects of City Layout in Gang Territorial Formations

**Damla Ortaç<sup>1</sup>**

**Supervisor(s): Martin Skrodzki<sup>1</sup>, Alethea Barbaro<sup>1</sup>**

<sup>1</sup>EEMCS, Delft University of Technology, The Netherlands

A Thesis Submitted to EEMCS Faculty Delft University of Technology,  
In Partial Fulfilment of the Requirements  
For the Bachelor of Computer Science and Engineering  
June 25, 2023

Name of the student: Damla Ortaç

Final project course: CSE3000 Research Project

Thesis committee: Martin Skrodzki, Alethea Barbaro, Joana P. Gonçalves

An electronic version of this thesis is available at <http://repository.tudelft.nl/>.

# Effects of City Layout in Gang Territorial Formations

D. Ortaç

Delft University of Technology  
Faculty of Electrical Engineering, Mathematics and Computer Science  
The Netherlands

---

## Abstract

*Gang-related violence poses a significant challenge in numerous countries across the world. While previous research have explored modeling formation of gang territories, none of them incorporated a city layout such as roads, water bodies and parks while doing so. Hence, this research explores the effects of city layout in the formation of gang territories. First the effects of a single vertical boundary of varying permeability is observed. Following this, the model is applied to real world where a part of Chicago's city layout is incorporated to the model. The results are then compared to gang territory maps shared by Chicago Police Department. The experiments show that city layout significantly affects the shape and size of the territories. By fine tuning the permeability for different terrain features, we can observe that the territories produced by the model show resemblance to their real world counterparts.*

---

## 1. Introduction

Gang related violence is a prominent problem in many countries. Up to 19 percent of all homicides recorded globally in 2017 were related to organized crime and gangs according to United Nations Office on Drugs and Crime [Uni15]. This equates to an average of roughly 65,000 killings every year. Due to their significant contribution to local crimes, it is important to understand the formation of gang territories.

Many of these gangs differentiate themselves via their unique graffiti markings that they leave across their territories [Bed18]. There have been several research papers on the formation of gang territories based solely on their graffiti markings [AB18, AB21, LC74, JLJ09]. However, in reality the borders of the territories may be affected by many other factors including the city layout. With the purpose to fill this void in crime modeling research, this paper aims to tackle the research question: "How does the city layout affect the formation of gang territories?". It explores the effects of incorporating city layout to the territorial formations of gangs based on the hypothesis that both natural formations (lake, rivers, hills etc.) and man-made structures (blocks, highways, city boundaries etc.) can effectively shape the boundaries where one gang's territory ends and another begins.

Considering the gangs' significant contribution to local crimes, this research can be a starting point for gaining a more realistic understanding of the formation of such territories. Furthermore, it can offer guidance to police force with managing inter-gang violence considering that gang violence, including homicide, is most often directed against other gang members [DP10]. The ethical considerations of this is further discussed in section 6.

In this paper, first, the scientific background is provided in section 2 followed by the related work on modelling gang territories and geographical terrain 3. Next, the research methodology will be discussed in section 4. Then the results will be shown and discussed in section 5, followed by the responsible research analysis in section 6. Finally, the research will be concluded in section 7.

## 2. Background

This paper refers to several scientific concepts which will be summarized and explained in this section.

### 2.1. Convection-Diffusion Model

A convection-diffusion model describes the transfer of particles, energy, or other physical quantities within a physical system, occurring through two mechanisms: convection and diffusion. Convection is the process in which heat moves through a gas or a liquid as the hotter part rises and the cooler, heavier part sinks [Hor10a]. Diffusion is the act of spreading something widely in all directions [Hor10b].

An order parameter is a measure of the degree of order across the boundaries in a phase transition system [CHK\*94]. In this paper, an order parameter analysis is used to observe how changing parameters of the model effect phase transitions.

### 2.2. Lattice Random Walker Model

The random walk theory is based off of the Brownian motion. This motion was studied to explain the irregular motion of individual

pollen particles by Robert Brown [Bro28]. The term random walk was first introduced by Karl Pearson in 1905 and it describes a path of a particle or an "agent" that consists of a succession of purely random steps on a mathematical space [PEA05]. In a biased random walk on the other hand, the probabilities of the potential succeeding steps are unequal. This can be due to a repellent or an attractant factors present on the neighboring cells. In this paper, the model is a biased random walker model.

The set of neighboring cells can also be different from model to model. In this paper, the particles can only move within their von Neumann neighborhood or to the four cells residing directly above, below, left or right of their current cell [Zai17].

Random walker models can also have different boundary conditions. The two that are relevant for this paper are periodic and hard-wall boundary conditions. Periodic boundary conditions are used to create a representation of an toroidal space with a finite 2-dimensional lattice. A toroidal space is a hollow circular ring. An example of this can be seen in figure 2. Any particle that reach the boundary of the lattice appears on the opposing side of the lattice creating an infinite chance of moving in one direction. In hard-wall boundary conditions, when a particle reaches the edge of the lattice, it will have a limited number of moves instead. It will not be able to extend it's move past the boundaries of the lattice, creating a finite space.

In figure 1 the arrows showcase the possible movements of the agents based off of their von Neumann neighborhoods. The image on the left depicts a hard-wall boundary condition while the one on the right depicts a periodic boundary condition.

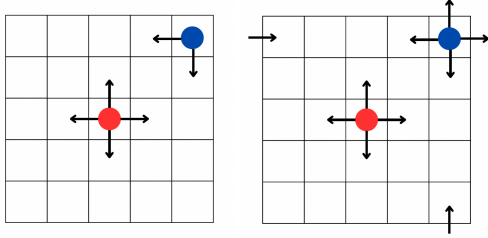


Figure 1: On the left agents on a hard-wall boundary lattice, on the right agents on a periodic boundary lattice



Figure 2: A toroidal object

### 3. Related Work

#### 3.1. Modeling of Gang Territory

As mentioned in the introduction, there have been several published research papers on the formation of gang territories based on their graffiti markings. The paper "A convection–diffusion model for

gang territoriality" even modelled the territorial segregation based on the repellent effect of other gang's graffiti markings [AB18]. This paper and the associated model will be referred to as "the existing model" and "the existing paper" in the rest of this paper.

The existing model is a biased random walk model where the mathematical space is a spatially uniform 2-dimensional lattice [AB18]. The agents represent gang members and these agents can only move to cells within the von Neumann neighborhood of the cell they reside in. The bias in the random walk is created by a repellent force applied via graffiti markings. Each gang member has a chance of depositing a graffiti marking on the cell they currently reside in at each time step with a probability of  $\gamma$ . Deposited graffiti markings decay with a rate of  $\lambda$ . The density of graffiti,  $\xi_i$  at a given cell with coordinates  $(x,y)$ , at time  $t + \delta t$  can be calculated as:

$$\xi_i(x,y,t + \delta t) = \xi_i(x,y,t) - (\lambda \cdot \delta t) \cdot \xi_i(x,y,t) + (\gamma \cdot \delta t) \cdot \rho_i(x,y,t)$$

where  $\delta t$  represents the length of each time step, and  $\rho_i(x,y,t)$  represents the agent density at cell  $(x,y)$  and time  $t$ .

The amount of repellent present at a given cell affects the probability of any agent at any neighboring cell to move onto said cell. The movement of an agent from cell  $(x_1,y_1)$  to  $(x_2,y_2)$  follows the equation:

$$M_a(x_1 \rightarrow x_2, y_1 \rightarrow y_2, t) = \frac{e^{-\beta \xi_B(x_2, y_2, t)}}{\sum_{(\tilde{x}, \tilde{y}) \sim (x_1, y_1)} e^{-\beta \xi_B(\tilde{x}, \tilde{y}, t)}}$$

where  $\beta$  is a parameter that controls the strength of avoidance of the other gang's graffiti, and  $(\tilde{x}, \tilde{y}) \sim (x_1, y_1)$  represents the neighbors of the cell  $(x_1, y_1)$ .

While this model doesn't incorporate city layout in the movement of the agents, it provided a base model that can be easily extended to do so.

#### 3.2. Modeling the Effects of Geographical Terrain on Territorial Behavior

In several other research papers we can see the incorporation of geographical terrain when modeling territorial behavior of pact animals such as wolves and coyotes [MLC06, KBSA07]. Furthermore, there are several other research papers that focus on similar effects of the medium on bacterial territory formations [ATG\*22]. All these models showcase that there is a significant effect of terrain features on the location and shape of the territories. Due to this, it is fair to assume a similar significant effect in the gang territorial formations as well.

### 4. Methodology

The research introduced in this paper consists of various steps. First, the existing mathematical model is extended to allow for the terrain to be a deciding factor. Then, a computational model that represents this mathematical model is created. Finally the results of the model are compared both quantitatively and qualitatively against the existing model and qualitatively against the actual gang territory maps from various cities.

#### 4.1. Mathematical Model

The model explored in this paper keeps the same graffiti production and decay equation as the existing model [AB18]. However the movement equations have been altered to also include a component called "hardness". Each lattice cell is given a hardness value between 0 and 1 with the function  $h$  where  $h(x,y)$  gives the hardness value at cell  $(x,y)$  on the lattice. The hardness inversely effects the chances of an agent to move on to said cell with factor  $\alpha$  following the equation:

$$M_a(x_1 \rightarrow x_2, y_1 \rightarrow y_2, t) = \frac{e^{-\beta \xi_B(x_2, y_2, t) - \alpha h(x_2, y_2)}}{\sum_{(\tilde{x}, \tilde{y}) \sim (x_1, y_1)} e^{-\beta \xi_B(\tilde{x}, \tilde{y}, t) - \alpha h(x_2, y_2)}}$$

This hardness component represents a physical boundary. As mentioned in the introduction, in the applied case, this boundary will be representing the city layout where streets, highways etc. would have higher hardness values then other areas.

The  $\alpha$  value represents the overall importance of the hardness similar to the  $\beta$  value that represents the overall importance of the graffiti repellence in the motion of the agents. Since the  $\beta$  value is thoroughly explored in the existing paper, this paper will focus on the  $\alpha$  value.

To simplify mathematical analysis, during the order parameter analysis in section 4.3.1.2 the hardness will be kept to 1 when there is a boundary, and 0 otherwise. This is to solely focus on the critical value for  $\alpha$  as mentioned. However when the model will be applied to a real city, the  $\alpha$  value will be kept constant and hardness value will differ based on the type of boundary. This process is further explained in section 4.3.2.

#### 4.2. Computational Model

The computational model represents the mathematical model mentioned in section 4.1. However, the lattice has hard-wall boundaries instead of the periodic boundaries of the existing model, meaning that agents at the edges of the lattice have limited number of movement options. This choice is made to create a closer representation of a real obstacle since an agent shouldn't be able to move away from a boundary and appear behind it.

To simplify the process of reading hardness value of each cell, a pipeline way created that turns basic map images into matrices of RGB colors of the image. This is then converted into a matrix that acts as a lookup table for the hardness of each cell. This is calculated so black pixels with RGB values (0, 0, 0) have hardness 1, white pixels with RGB values (255, 255, 255) have hardness 0 and other colored pixels can have a value between 0 and 1 depending on their red, blue, and green components and the factors ranging from 0 to 1 assigned to each respectively, following the equation:

$$H(x,y) = \frac{R(x,y)}{255} \cdot f_R + \frac{G(x,y)}{255} \cdot f_G + \frac{B(x,y)}{255} \cdot f_B.$$

where  $R(x,y)$ ,  $G(x,y)$ , and  $B(x,y)$  represent the red, green and blue component of the image at cell  $(x,y)$  respectively.  $f_R$ ,  $f_G$ , and

$f_B$  represents the hardness factor of red, green, and blue components respectively.

This allows for black pixels to represent out of reach areas, white pixels to represent no obstacle in cell and other colors to represent a different type of obstacle.

#### 4.3. Result Comparison

As previously mentioned the results of the new model will be compared to the existing model and real gang territory maps in cities.

##### 4.3.1. Comparison with the Existing Model

**4.3.1.1. Observing the Effects of Hard-Wall Boundaries** Before any comparison could be done with obstacles, it is necessary to observe the sole effect of changing the periodic boundaries to hard wall boundaries. To achieve this, the parameters of the extended model are kept equal to the results shown in the existing paper where  $N_A = N_B = 100,000$  with  $\lambda = \gamma = 0.5$ ,  $\beta = 2 \cdot 10^{-5}$ ,  $\delta t = 1$  and the lattice size is 100 by 100 [AB18]. Then the results of running this model for 0, 1000, 10000, and 200000 iterations are compared. The results from existing paper can be found in figure 5.

**4.3.1.2. Observing the Effects of Single Vertical Boundary** To make a quantitative comparison the model is run on a simple map with a single vertical obstacle down the center of the 100x100 lattice. Since 100 cells don't have an exact center, the center right column is chosen. An example of this in a 10 by 10 matrix can be found in figure 3.

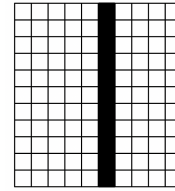


**Figure 3:** A 10 by 10 matrix with a single vertical boundary down the center right

When the existing model is simulated two possible states are observed: a well-mixed state where agents and graffiti of both colors are uniformly distributed throughout the lattice and a well-segregated state where red agents and red graffiti separate from blue agents and blue graffiti [AB18]. In the extended model, it is expected that the well-segregated state will now split into two states based on if the territories on either side of the boundary are matching or not.

In this section, we explore these three possible phases for our model, defining an order parameter to quantify the distinction between them. To make the comparison two different order parameters are considered.

$$\epsilon_1(t) = \left( \frac{1}{NL} \right) \sum_{(x,y) \in H} |(\rho_A(x,y-1,t) - \rho_B(x,y-1,t)) - (\rho_A(x,y+1,t) - \rho_B(x,y+1,t))|$$

$$\varepsilon_2(t) = \left( \frac{1}{4N^2L} \right) \sum_{(x,y) \in H} (\rho_A(x,y-1,t) - \rho_B(x,y-1,t)) \cdot (\rho_A(x,y+1,t) - \rho_B(x,y+1,t))$$

where  $H$  is the set of lattice squares that have a hardness value of 1. Thus the order parameters only consider the cells on the immediate left and right of the boundary.

After careful consideration, the second order parameter,  $\varepsilon_2$  is chosen due to its proximity to the order parameter used in the existing model's  $\beta$  analysis as well as the classic Ising Model, a mathematical model of ferromagnetism in statistical mechanics [AB18, Isi25]. The resultant value of the term inside summation is positive if the sites on either side of the boundary are dominated by the same color, and negative if they are dominated by the opposite colors. The coefficient at the front normalizes the sum.

This section will only contain the exploration of the boundaries of the chosen order parameter,  $\varepsilon_2$ , however the detailed analysis of the boundaries of the other order parameter,  $\varepsilon_1$  can be found in Appendix A.

The existing paper provides a proof to why the expected agent density at each cell is approximately  $N_A$  and  $N_B$  respectively during the well-mixed state [AB18]. Since this state does not change between the models we can assume this approximation as well. Following this, for the well-mixed state at  $t = 0$  we can approximate the  $\varepsilon_2$  value:

$$\varepsilon_2(0) = \left( \frac{1}{4N^2L} \right) \sum_{(x,y) \in H} (N_A - N_B) \cdot (N_A - N_B)$$

If we begin with  $N_A = N_B$ , then:

$$\begin{aligned} \varepsilon_2(0) &= \left( \frac{1}{4N^2L} \right) \sum_{(x,y) \in H} (0) \cdot (0) \\ &= 0 \end{aligned}$$

This means that at the well-mixed state the order parameter  $\varepsilon_2$  should have a value close to 0.

In the segregated state, we have to consider two conditions. When alpha is low, the boundary becomes more permeable and territories are more likely to continue across the border. This makes it more likely that the cells on either side of the border be dominated by the same gang. In other words, cells on either side of the border contain more of the same type of gang's agents and graffiti.

By assuming that in the fully segregated state every cell is dominated by either one of the gangs and the two gangs have equal dominated area as shown in the existing paper [AB18], we can split the order parameter as follows:

$$\begin{aligned} \varepsilon_2(t) &= \left( \frac{1}{4N^2L} \right) \sum_{(x,y) \in H_A} (\rho_A(x,y-1,t) - \rho_B(x,y-1,t)) \cdot (\rho_A(x,y+1,t) - \rho_B(x,y+1,t)) \\ &\quad + \left( \frac{1}{4N^2L} \right) \sum_{(x,y) \in H_B} (\rho_A(x,y-1,t) - \rho_B(x,y-1,t)) \cdot (\rho_A(x,y+1,t) - \rho_B(x,y+1,t)) \end{aligned}$$

where  $H_A$  and  $H_B$  is the set of lattice squares that have a hardness value of 1 and are dominated by gang A and B respectively. We can assume that for low alpha values, even on the boundary either one of the gangs will be dominating every cell since the permeability will be high. Then we can say that  $H = H_A + H_B$ .

The existing paper estimates the agent density at a cell during the segregated state to be  $2N_A$  and  $2N_B$  respectively for cells within the territory of gang A and B and 0 in the opposing gang's territory [AB18] which can also be applied to this order parameter:

$$\begin{aligned} \varepsilon_2(t) &= \left( \frac{1}{4N^2L} \right) \sum_{(x,y) \in H_A} (2N_A - 0) \cdot (2N_A - 0) \\ &\quad + \left( \frac{1}{4N^2L} \right) \sum_{(x,y) \in H_B} (0 - 2N_B) \cdot (0 - 2N_B) \\ &= \left( \frac{1}{4N^2L} \right) \left( \sum_{(x,y) \in H_A} 4N_A^2 + \sum_{(x,y) \in H_B} 4N_B^2 \right) \end{aligned}$$

Assuming starting with  $N_A = N_B = N$  and the boundary is split approximately equally between the two territories where  $|H_A| = |H_B| = \frac{|H|}{2}$ . Note that  $|H| = L$  since it is a vertical line passing through the map, thus we get:

$$\begin{aligned} \varepsilon_2(t) &= \left( \frac{1}{4N^2L} \right) \left( \sum_{(x,y) \in H_A} 4N^2 + \sum_{(x,y) \in H_B} 4N^2 \right) \\ &= \left( \frac{1}{4N^2L} \right) \sum_{(x,y) \in H} 4N^2 = \left( \frac{1}{4N^2L} \right) \cdot L \cdot 4N^2 \\ &= 1 \end{aligned}$$

On the other hand, when alpha value increases, the boundary becomes more opaque letting less agents pass to the other side. In this case, for high alpha values the different sides of the border act like two independent lattices hence the chance of cells on either side of the border be dominated by the same gang becomes independent. Due to this, the order parameter value should lie in between 0 and 1 with a normal distribution for high alpha values.

The model is run as ensembles of 100 for each set of parameters. Parameters  $N_A = N_B = 50,000$ ,  $\lambda = \gamma = 0.5$ ,  $\beta = 3 \cdot 10^{-5}$ ,  $\delta t = 1$  are kept constant,  $\alpha$  is changed from 0 to 1 at 0.1 intervals as well as to 3 and 5 to observe the effect at larger values and the model is run for 100,000 time steps. The order parameter is calculated at each time step.

First, for each  $\alpha$ 's ensemble, order parameter values are averaged at each time step and are graphed against time. Then to smooth out the graph, a sliding window average with a window size of 100 time steps is plotted against time. Finally box and whisker plots are created for each alpha value.

Finally, a one-way ANOVA analysis [RWRW17] is performed in the final order parameter values of each  $\alpha$  pair to determine threshold alpha value, where larger values don't make a statistically significant difference in the final order parameter value.

**4.3.1.3. Observing the Effects of Halving Lattice Size** As mentioned in section 4.3.1.2, for high alpha values, either side of the boundary behaves like two 100 by 50 matrices. To assure that such a size downgrade and the non-square lattice doesn't significantly affect the patterns formed, the model is run with 100 by 50 matrix with no obstacles added. The parameters are kept constant to the hard-wall boundary run where  $N_A = N_B = 50,000$ ,  $\lambda = \gamma = 0.5$ ,  $\beta = 2 \cdot 10^{-5}$ ,  $\delta t = 1$  for 200000 time steps for easy comparison.

### 4.3.2. Comparison with Real City Maps

As an example city, Chicago is chosen. There are several factors affecting this choice. First of all, Chicago has a very prominent gang presence, where most of the city grounds are indeed a territory of gangs. Since the model introduced in this paper, initializes with gang presence at the entirety of the map, this extensive prominence would allow for a more direct comparison. Secondly, crime maps, including gang territory maps, are hard to obtain due to several privacy and security concerns [WM01]. However, the Chicago Police Department has publicly available gang territory maps from various years [Chi]. Finally, the city of Chicago contains varying types of obstacles in a small area. There are roads, parks, lake and a river in close proximity to each other, allowing for testing the model on combination of varying hardness.

First a map of Chicago is obtained via Google Maps [Goo]. Then the map is simplified by reducing the density of features using the tools offered. This omitted the local roads, and all landmarks aside from parks and forests. The exact configuration and area used can be found in Appendix B. Then, using the same tool, the assigned colors of the roads, parks, water bodies and background are changed to desired colors and the size is reduced to 200x200 pixels. The map can be found in figure 4 on the left.

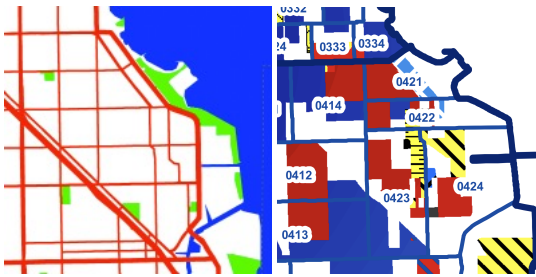


**Figure 4:** On the right the simplified and color-coded city layout map, on the left the same area as the city layout from the Chicago PD gang territory map of 2022 [Chi]

Following this, first an RGB matrix is created from this simplified map. Then, a hardness matrix is created with the formula introduced in section 4.2 where  $f_R = 0.75$ ,  $f_G = 0.85$ , and  $f_B = 0.95$  using the RGB matrix. These factors are chosen with the intention of mimicking the real permeability of these features in mind. Water bodies are not passable unless there is a ferry system or bridges available, neither of which is present in Chicago and thus the factor is chosen to be 1.0. Public parks and forest areas are still permeable however the maps provided by Chicago PD showed no gang dominance in these areas so they are given a factor of 0.85. Finally roads should be the most permeable out of all three, but still should be hard enough to separate the territories and thus is given a factor of 0.75.

The model is run with parameters  $N_A = N_B = 100,000$  with  $\lambda = \gamma = 0.5$ ,  $\beta = 2 \cdot 10^{-5}$ ,  $\delta t = 1$  and the lattice size is 200 by 200 for 20.000 time steps with several alpha values on and around the threshold determined from the ANOVA analysis.

Then the results will be compared to the same chosen area of the published map of the gangs' territories in the Chicago PD website [Chi]. It is extremely important to address the difference between the behavior of real life gangs and the model gangs before any comparison can be made. In the creation of a real life gang's territory, the size of the gang population increases starting from a specific point and depending on the competition with other gangs and police force, it expands into a larger area and grows in size or shrinks and eventually disappears. Our model doesn't represent such a behavior, it only focuses on the shapes of the territories. Thus, there is no relevant data to quantitatively compare results of the model against real cities with a prominent gang presence. Due to this, the comparison can solely be done qualitatively. The main comparison point will be the shapes of the edges of the territories. The exact area chosen can be found in 4 on the right, and the full map with a legend of the exact gangs each shading represent can be found in Appendix C.

## 5. Results and Discussion

### 5.1. Effects of Hard-Wall Boundary

As the hard-wall boundary results are compared to the images from the existing paper, the only change on the overall segregation that is observed is that the territories do not wrap around periodically but rather end in the boundaries as expected. However there is not a significant effect on the territory sizes and overall shapes. This means that any discrepancies between the existing model and the model introduced in this paper's result sizes and shapes when the obstacles are added majorly depend on the addition of the obstacles and not the boundary conditions. Results of the introduced model and existing model can be found in figures 6 and 5 respectively.

### 5.2. Effects of Lattice Size

As mentioned in section 4, the model acts as two independent lattices on either side of the boundary for high  $\alpha$  values. This raised a concern regarding if the behavior of the gangs would change due to the halved size of the lattice. However, as seen in figure 7, the emerging patterns when the model is run on a 50 by 100 lattice does

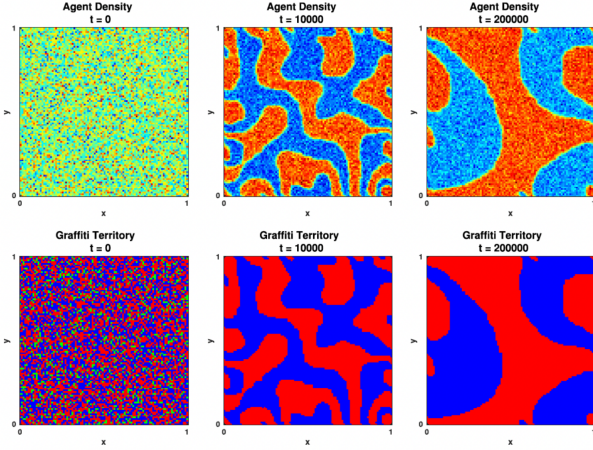


**Figure 5:** Results of the 0th, 10000th and 200000th iterations of the existing model run with parameters  $N_A = N_B = 100,000$  with  $\lambda = \gamma = 0.5$ ,  $\beta = 2 \cdot 10^{-5}$ ,  $\delta t = 1$  on a 100 by 100 lattice [AB18]

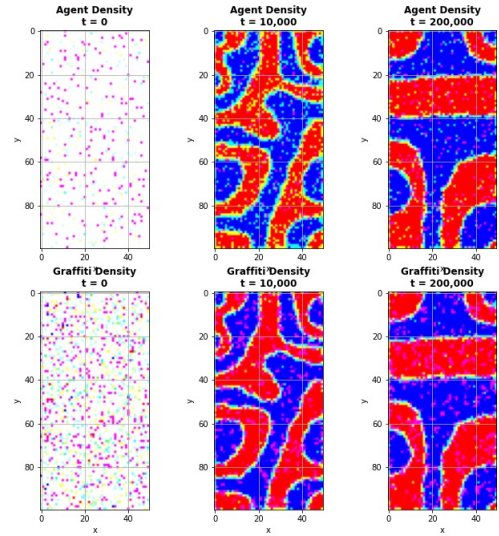


**Figure 7:** Results of the 0st, 10000th and 200000th iterations of the existing model run with parameters  $N_A = N_B = 100,000$  with  $\lambda = \gamma = 0.5$ ,  $\beta = 2 \cdot 10^{-5}$ ,  $\delta t = 1$  on a 100 by 50 lattice

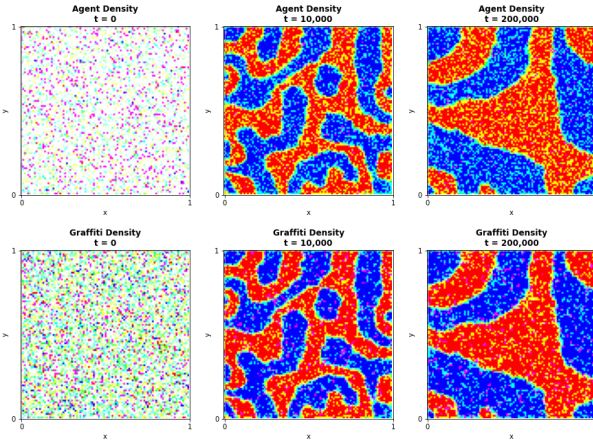


**Figure 6:** Results of the 0th, 10000th and 200000th iterations of the model introduced in this paper run with parameters  $N_A = N_B = 100,000$  with  $\lambda = \gamma = 0.5$ ,  $\beta = 2 \cdot 10^{-5}$ ,  $\delta t = 1$  on a 100 by 100 lattice

not differ from a 100 by 100 lattices patterns seen in figures 6 and 5. The territories still have round edges, and have similar girths in same time steps.

### 5.3. Effects of Single Vertical Boundary

After it is determined that any observed differences between the single vertical boundary runs and regular runs will be due to the addition of boundary, single vertical boundary runs for several alpha values are compared. Figure 8 showcases how order parameter value changed with time for a selected number of alpha values.

As expected from the order parameter boundary analysis, the order parameter value starts close to 0 for all alpha values. For  $\alpha = 0$ , the final order parameter value is close to 1 and the final value ranges

between 1 and 0 for all higher alpha values. The plots show a logarithmic regression in the order parameter values with time step. However due to the rapid variations in the order parameter value, and how close the values are for some alpha values, it is very difficult to visually analyze the results further then this.

The sliding window averaged version of the same plot can be found in figure 9. Here, the plots smoothen out and the effects of varying alpha values can be observed better. It is important to note that the first 99 time steps are omitted due to the sliding window size of 100. This is why, the plots appear to start at values significantly larger then 0.

Focusing on the final order parameter values, it is observed that alpha values between 0 and 0.4 all appear in order where 0 results in the highest and 0.4 results in the lowest value. However for values larger then 0.4, the lines no longer follow the same order, and appear very closely to each other, overlapping at times. No further deductions could be made from the plots.

To analyze the results further, a box and whisker plot for the final order parameter values of each trial for each alpha value are drawn and can be seen in 10. Here it appears that final order parameter values for alpha values of 0.5 and higher all mostly overlap.

To statistically show that the order parameter behaviour is different up to alpha value of 0.5, a one-way ANOVA analysis is performed on the final order parameter values of each alpha value excluding the outliers marked as red dots on the box and whisker plot found in 10. The outliers are excluded due to the assumption that these are due to the innate randomness of the model and would hinder the significance of the statistical analysis. Table 1 showcases the p values for

all  $\alpha$  pairs. A p value less than 0.05 indicates a statistically significant difference between the final order parameter value ensembles of the  $\alpha$  pair. From the table we can see that values between 0 and 0.4 all show a statistical significance to all other values with the exception of 0.3 and 0.4 pair. The exceptions could be due to the randomness in the model's behavior as mentioned before. For ensemble sizes larger than 100, such randomness can be decremented however will never be entirely omitted. From this, we can make a conclusion that there appears to be an  $\alpha$  value between 0.4 and 0.5 before which there is a statistically significant difference for differing  $\alpha$  values.

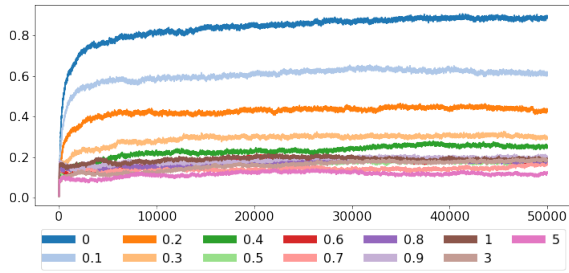


Figure 8: Order parameter vs. time for various  $\alpha$

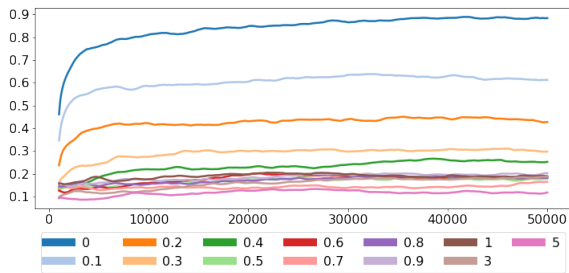


Figure 9: Order parameter vs. time for various  $\alpha$  values that are smoothed by taking a sliding window average of 100 time steps

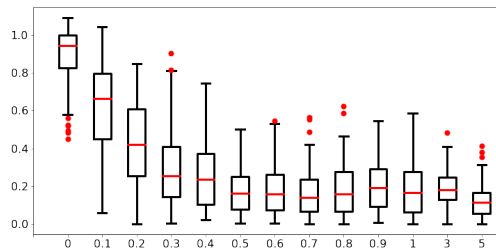


Figure 10: Order parameter vs.  $\alpha$  in the form of box and whisker plots

### 5.4. Real World Application

As previously mentioned, in figure 4, the map on the right shows the real gang territories in the chosen area of Chicago in 2022. This is compared to the results of the model runs with a hardness matrix mimicking the city layout in the same figure, figure 4 on the left. In section 5.3, it is concluded that a statistically significant effect in the results are only observed when increasing  $\alpha$  value from 0 to 0.4 indicating a threshold between 0.4 and 0.5. Due to this, the model applied to Chicago's city layout are run on  $\alpha$  values of 0.35, 0.45, and 0.65 to observe how the model behaves below, above and on the threshold. The results can be found in figures 11, 12 and 13 respectively. It is expected that the territories will get segregated between the boundaries existing in the city layout as the real world data suggests in figure 4 on the right, and the segregation would be more in 0.45 and 0.65 compared to 0.35. There should also be no significant difference between the results of  $\alpha$  values 0.45 and 0.65. The results indeed follow these expectations. It can be observed that no agents pass on to the lake, and the river extending from the lake on the right bottom corner is only passed via the existing bridge due to the bright green indicating lack of agents and graffiti. The two gang types, indicated with red and blue in the map, appear to be segregated with the roads. The rectangular areas carved between roads mostly appear to be a singular gang type for the  $\alpha$  values of 0.45, and 0.65 while this effect is less present in 0.35 where territories tend to span multiple areas indicating that roads are more permeable. Also the shapes of the territories in the result of  $\alpha = 0.35$  are more circular and don't match the shapes carved by the obstacles.

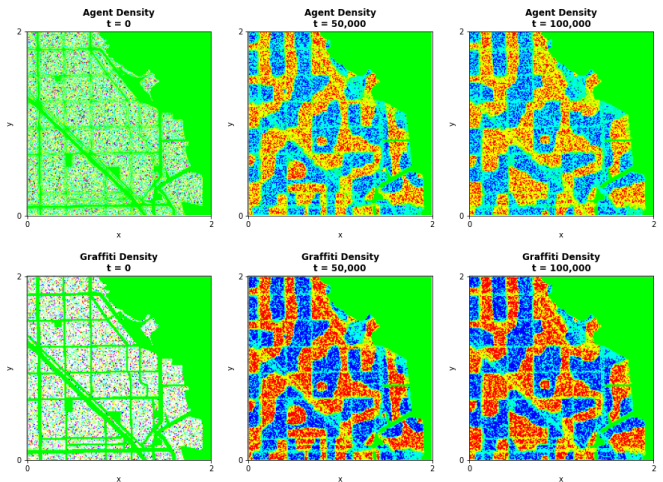


Figure 11: Model applied to Chicago city layout with  $\alpha$  value of 0.35

## 6. Responsible Research

### 6.1. Accessibility

It is crucial in research to make sure that other researchers can independently confirm and reproduce the findings. To ensure the reproducibility of this study, the source code is publicly accessible on

$\alpha$	0	0.1	0.2	0.3	0.4	0.5	0.6	0.7	0.8	0.9	1	3	5
0	X	0	0	0	0	0	0	0	0	0	0	0	0
0.1	0	X	0	0	0	0	0	0	0	0	0	0	0
0.2	0	0	X	0	0	0	0	0	0	0	0	0	0
0.3	0	0	0	X	0.111	0	0	0	0	0	0	0	0
0.4	0	0	0	0.111	X	0.001	0.001	0	0.002	0.018	0.003	0.001	0
0.5	0	0	0	0	0.001	X	0.932	0.672	0.841	0.24	0.66	0.53	0.001
0.6	0	0	0	0	0.001	0.932	X	0.74	0.78	0.214	0.605	0.477	0.001
0.7	0	0	0	0	0	0.672	0.74	X	0.549	0.117	0.399	0.278	0.004
0.8	0	0	0	0	0.002	0.841	0.78	0.549	X	0.354	0.822	0.711	0.001
0.9	0	0	0	0	0.018	0.24	0.214	0.0117	0.354	X	0.476	0.489	0
1	0	0	0	0	0.003	0.66	0.605	0.399	0.822	0.476	X	0.907	0
3	0	0	0	0	0.001	0.53	0.477	0.278	0.711	0.489	0.907	X	0
5	0	0	0	0	0	0.001	0.001	0.004	0.001	0	0	0	X

Table 1: One-way ANOVA analysis on all  $\alpha$  pair's final order parameter values

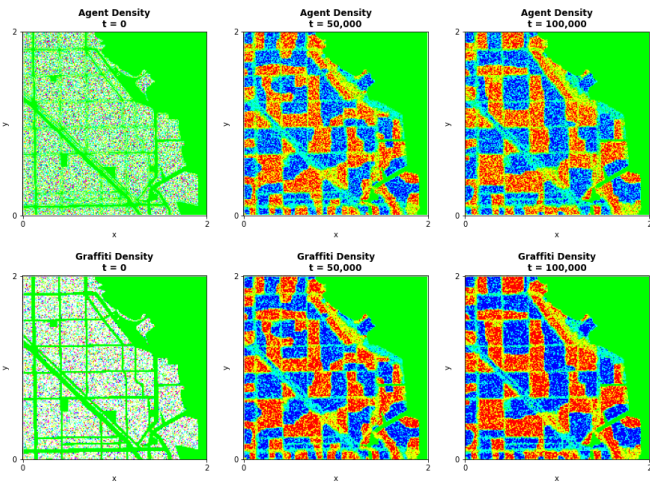


Figure 12: Model applied to Chicago city layout with  $\alpha$  value of 0.45

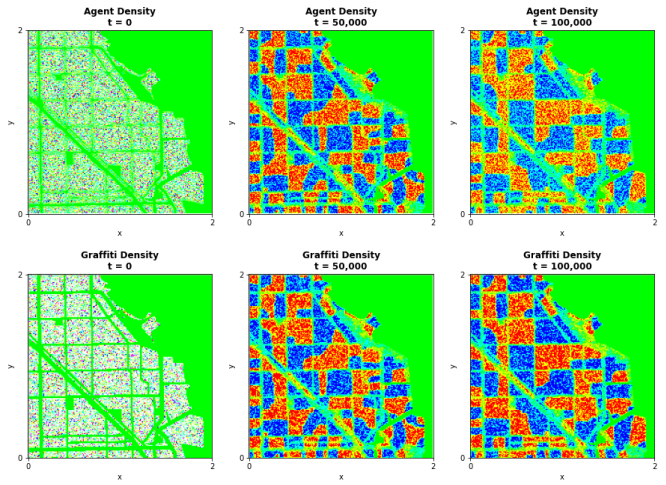


Figure 13: Model applied to Chicago city layout with  $\alpha$  value of 0.65

GitHub under the username "damlaortac", accompanied by comprehensive documentation delineating the procedures for executing the model. Moreover, the code has no special hardware dependency and can be executed on most modern computer systems.

### 6.2. Ethical Concerns

With most research on crime modeling there always are some ethical concerns regarding the use of the outcome from the model in real life situations in the form of predictive policing. As Andre A. Norton describes: "Predictive policing is a concept that is built on the premise that it is possible to predict when and where crimes will occur again in the future by using sophisticated computer analysis of information about previously committed crimes" [Nor13]. While predictive policing can be beneficial in preventing crime and reducing the load on police forces, due to the personal data used as input, it comes with a lot of privacy concerns, discriminatory decisions and lack of accuracy and accountability [MW19]. In the case of the model represented in this paper however, since it is a theory driven

model rather than a data driven model, these concerns are not relevant. The model does not take any pre-existing gang data to make predictions. Due to this, this model can only be a starting point for gaining a more realistic understanding of the formation of such territories in the context of various cities and can offer guidance to police force regarding inter-gang interactions.

### 7. Conclusion and Future Work

The aim of this paper was to investigate the effects of city layout in the formation of gang territories. Effects of terrain has been found to be relevant when modeling territorial animals yet research on gang territories lack such incorporation. Hence, the effects of adding a vertical boundary with varying permeability was explored. Following this, the outcome of this experiment was used in applying the model to real world, where the model was run on a part of Chicago's city layout and the results are compared to a gang territory map shared by Chicago Police Department.

Based on comparisons of the results against the results of preced-

ing research, incorporating various elements of city layouts such as roads, lakes, and parks significantly affect the shapes and size of gang territories. And by adjusting the permeability of such boundaries within our model, we can bring the model closer to real world scenarios where gang territories do show resemblance to the terrain of the neighborhood they reside in as well as the real gang territories found in the same neighborhood.

During the study several future research directions came to light. It would be interesting to observe if the gangs' formation is effected by the location of institutions such as police departments, schools, hospitals. For example close proximity to police force may be a negative influence in the growth of gangs' territory. It would also be interesting to explore if the natural terrain would have an effect on the territory shapes and location. It would be interesting if gang's prefer to form in higher land which may be seen as vantage point. Finally, it would also be a intriguing to see how the territories behave with similar city layouts when the number of gang types increase. The computational model introduced in this paper was written for multi-species, however was only used to observe two gang types, which could be a great starting ground for such research. The public codebase of the model named "GangTerritory" can be found on GitHub under the user "damlaortac".

## References

- [AB18] ALSENAFI A., BARBARO A. B.: A convection–diffusion model for gang territoriality. *Physica A: Statistical Mechanics and its Applications* 510 (Nov. 2018), 765–786. URL: <https://doi.org/10.1016/j.physa.2018.07.004>, doi:10.1016/j.physa.2018.07.004. 1, 2, 3, 4, 6
- [AB21] ALSENAFI A., BARBARO A.: A multispecies cross-diffusion model for territorial development. *Mathematics* 9, 12 (June 2021), 1428. URL: <https://doi.org/10.3390/math9121428>, doi:10.3390/math9121428. 1
- [ATG\*22] ASP M. E., THANH M.-T. H., GERMANN D. A., CARROLL R. J., FRANCESKI A., WELCH R. D., GOPINATH A., PATTESON A. E.: Spreading rates of bacterial colonies depend on substrate stiffness and permeability. *PNAS Nexus* 1, 1 (Mar. 2022). URL: <https://doi.org/10.1093/pnasnexus/pgac025>, doi:10.1093/pnasnexus/pgac025. 2
- [Bed18] BEDORF F.: Bibliography. In *Sweet Home Chicago?* transcript Verlag, Dec. 2018, pp. 349–372. URL: <https://doi.org/10.1515/9783839441312-013>, doi:10.1515/9783839441312-013. 1
- [Bro28] BROWN R.: XXVII. ia brief account of microscopical observations made in the months of june, july and august/i 1827, ion the particles contained in the pollen of plants and on the general existence of active molecules in organic and inorganic bodies/i. *The Philosophical Magazine* 4, 21 (Sept. 1828), 161–173. URL: <https://doi.org/10.1080/14786442808674769>, doi:10.1080/14786442808674769. 2
- [Chi] URL: <https://gis.chicagopolice.org/pages/gang-maps>. 5
- [CHK\*94] CLARKE J. B., HASTIE J. W., KIHNBORG L. H. E., METSELAAR R., THACKERAY M. M.: Definitions of terms relating to phase transitions of the solid state (iupac recommendations 1994). *Pure and Applied Chemistry* 66, 3 (1994), 577–594. URL: <https://doi.org/10.1351/pac199466030577> [cited 2023-06-25], doi:10.1351/pac199466030577. 1
- [DP10] DECKER S., PYROOZ D.: Gang violence worldwide: Context, culture, and country. *Small Arms Survey 2010: Gangs, Groups, and Guns* (01 2010), 128–155. 1
- [Goo] URL: <https://mapstyle.withgoogle.com/>. 5
- [Hor10a] HORNBY A. S.: Convection. In *Oxford Advanced Learner's Dictionary of Current English*. Oxford University Press, 2010. 1
- [Hor10b] HORNBY A. S.: Diffusion. In *Oxford Advanced Learner's Dictionary of Current English*. Oxford University Press, 2010. 1
- [Isi25] ISING E.: Beitrag zur theorie des ferromagnetismus. *Zeitschrift für Physik* 31, 1 (feb 1925), 253–258. URL: <https://doi.org/10.1007/bf02980577>, doi:10.1007/bf02980577. 4
- [JLJ09] JAIN A. K., LEE J.-E., JIN R.: Graffiti-id: matching and retrieval of graffiti images. In *Proceedings of the First ACM workshop on Multimedia in forensics* (2009), pp. 1–6. 1
- [KBSA07] KARLSSON J., BRØSETH H., SAND H., ANDRÉN H.: Predicting occurrence of wolf territories in scandinavia. *Journal of Zoology* 272, 3 (Apr. 2007), 276–283. URL: <https://doi.org/10.1111/j.1469-7998.2006.00267.x>, doi:10.1111/j.1469-7998.2006.00267.x. 2
- [LC74] LEY D., CYBRIWSKY R.: Urban graffiti as territorial markers. *Annals of the association of American geographers* 64, 4 (1974), 491–505. 1
- [MLC06] MOORCROFT P. R., LEWIS M. A., CRABTREE R. L.: Mechanistic home range models capture spatial patterns and dynamics of coyote territories in yellowstone. *Proceedings of the Royal Society B: Biological Sciences* 273, 1594 (Apr. 2006), 1651–1659. URL: <https://doi.org/10.1098/rspb.2005.3439>, doi:10.1098/rspb.2005.3439. 2
- [MW19] MEIJER A., WESSELS M.: Predictive policing: Review of benefits and drawbacks. *International Journal of Public Administration* 42, 12 (2019), 1031–1039. URL: <https://doi.org/10.1080/01900692.2019.1575664>, <https://doi.org/10.1080/01900692.2019.1575664>, doi:10.1080/01900692.2019.1575664. 8
- [Nor13] NORTON A. A.: Predictive policing: The future of law enforcement in the trinidad and tobago police service (tpps). *International Journal of Computer Applications* 62, 4 (2013). 8
- [PEA05] PEARSON K.: The problem of the random walk. *Nature* 72, 1865 (July 1905), 294–294. URL: <https://doi.org/10.1038/072294b0>, doi:10.1038/072294b0. 2
- [RWRW17] ROSS A., WILLSON V. L., ROSS A., WILLSON V. L.: One-way anova. *Basic and Advanced Statistical Tests: Writing Results Sections and Creating Tables and Figures* (2017), 21–24. 5
- [Uni15] UNITED NATIONS OFFICE ON DRUGS AND CRIME: Global study on homicide executive summary, July 2015. 1
- [WM01] WARTELL J., MCEWEN J. T.: *Privacy in the information age: A guide for sharing crime maps and Spatial Data*. U.S. Department of Justice, Office of Justice Programs, 2001. 5
- [Zai17] ZAITSEV D. A.: A generalized neighborhood for cellular automata. *Theoretical Computer Science* 666 (Mar. 2017), 21–35. URL: <https://doi.org/10.1016/j.tcs.2016.11.002>, doi:10.1016/j.tcs.2016.11.002. 2

**Appendix A: Boundary Analysis of Not Chosen Order Parameter**

The first order parameter,  $\varepsilon_1$ , the measurement considered is the difference of how dominant one gang type is over the other on either side of the boundary.

In  $\varepsilon_1$ , assuming the same expected density of  $N_A$  and  $N_B$  in each cell, we have a very similar initial state order parameter value:

$$\varepsilon_1(0) = \left( \frac{1}{NL} \right) \sum_{(x,y) \in H} |(N_A - N_B) - (N_A - N_B)|$$

If we begin with  $N_A = N_B$ , then:

$$\begin{aligned} \varepsilon_1(0) &= \left( \frac{1}{NL} \right) \sum_{(x,y) \in H} |(0) - (0)| \\ &= 0 \end{aligned}$$

This means that at the well-mixed state the order parameter  $\varepsilon_1$  should have a value close to 0.

In the well-segregated state for low alpha values we can also do a similar separation:

$$\begin{aligned} \varepsilon_1(t) &= \left( \frac{1}{NL} \right) \sum_{(x,y) \in H_A} |(\rho_A(x,y-1,t) - \rho_B(x,y-1,t)) \\ &\quad - (\rho_A(x,y+1,t) - \rho_B(x,y+1,t))| \\ &+ \left( \frac{1}{NL} \right) \sum_{(x,y) \in H_B} |(\rho_A(x,y-1,t) - \rho_B(x,y-1,t)) \\ &\quad - (\rho_A(x,y+1,t) - \rho_B(x,y+1,t))| \end{aligned}$$

If we then follow similar assumption for the expected values we can get:

$$\begin{aligned} \varepsilon_1(t) &= \left( \frac{1}{NL} \right) \sum_{(x,y) \in H_A} |(2N_A - 0) - (2N_A - 0)| \\ &\quad + \sum_{(x,y) \in H_B} |(0 - 2N_B) - (0 - 2N_B)| \\ &= \left( \frac{1}{NL} \right) \left( \sum_{(x,y) \in H_A} |0| + \sum_{(x,y) \in H_B} |0| \right) \\ &= 0 \end{aligned}$$

So the value of  $\varepsilon_1$  again approximates to 0 for small alpha values.

In the well-segregated state for high alpha values, the same behavior as  $\varepsilon_2$  can be expected where either side of the boundary behaves as two independent lattices and hence the chance of cells on either side of the border be dominated by the same gang becomes independent. So, the order parameter value should lie in between 0 and 1 with a normal distribution for high alpha values for  $\varepsilon_1$  as well.

**Appendix B: Chicago Map Configuration for Google Maps**

```
[
  {
    "elementType": "labels",
    "stylers": [
      {
        "visibility": "off"
      }
    ]
  },
  {
    "featureType": "administrative.neighborhood",
    "stylers": [
      {
        "visibility": "off"
      }
    ]
  },
  {
    "featureType": "landscape.man_made",
    "stylers": [
      {
        "visibility": "off"
      }
    ]
  },
  {
    "featureType": "landscape.natural",
    "stylers": [
      {
        "color": "#ffffff"
      },
      {
        "visibility": "on"
      }
    ]
  },
  {
    "featureType": "poi",
    "elementType": "labels.text",
    "stylers": [
      {
        "visibility": "off"
      }
    ]
  },
  {
    "featureType": "poi.attraction",
    "stylers": [
      {
        "visibility": "off"
      }
    ]
  },
  {
    "featureType": "poi.business",
    "stylers": [
```

```

    {
      "visibility": "off"
    }
  ],
},
{
  "featureType": "poi.government",
  "stylers": [
    {
      "visibility": "off"
    }
  ]
},
{
  "featureType": "poi.medical",
  "stylers": [
    {
      "visibility": "off"
    }
  ]
},
{
  "featureType": "poi.park",
  "stylers": [
    {
      "color": "#00f900"
    }
  ]
},
{
  "featureType": "poi.place_of_worship",
  "stylers": [
    {
      "visibility": "off"
    }
  ]
},
{
  "featureType": "poi.school",
  "stylers": [
    {
      "visibility": "off"
    }
  ]
},
{
  "featureType": "poi.sports_complex",
  "stylers": [
    {
      "visibility": "off"
    }
  ]
},
{
  "featureType": "road",
  "stylers": [
    {
      "color": "#ff2600"
    }
  ]
},
    ]
  },
  {
    "featureType": "road",
    "elementType": "labels.icon",
    "stylers": [
      {
        "visibility": "off"
      }
    ]
  },
  {
    "featureType": "road.arterial",
    "elementType": "labels",
    "stylers": [
      {
        "visibility": "off"
      }
    ]
  }
],
{
  "featureType": "road.highway",
  "elementType": "labels",
  "stylers": [
    {
      "visibility": "off"
    }
  ]
},
{
  "featureType": "road.local",
  "stylers": [
    {
      "visibility": "off"
    }
  ]
},
{
  "featureType": "transit",
  "stylers": [
    {
      "visibility": "off"
    }
  ]
},
{
  "featureType": "water",
  "stylers": [
    {
      "color": "#0433ff"
    }
  ]
}
]

```

Appendix C: Chicago Gang Territory Map

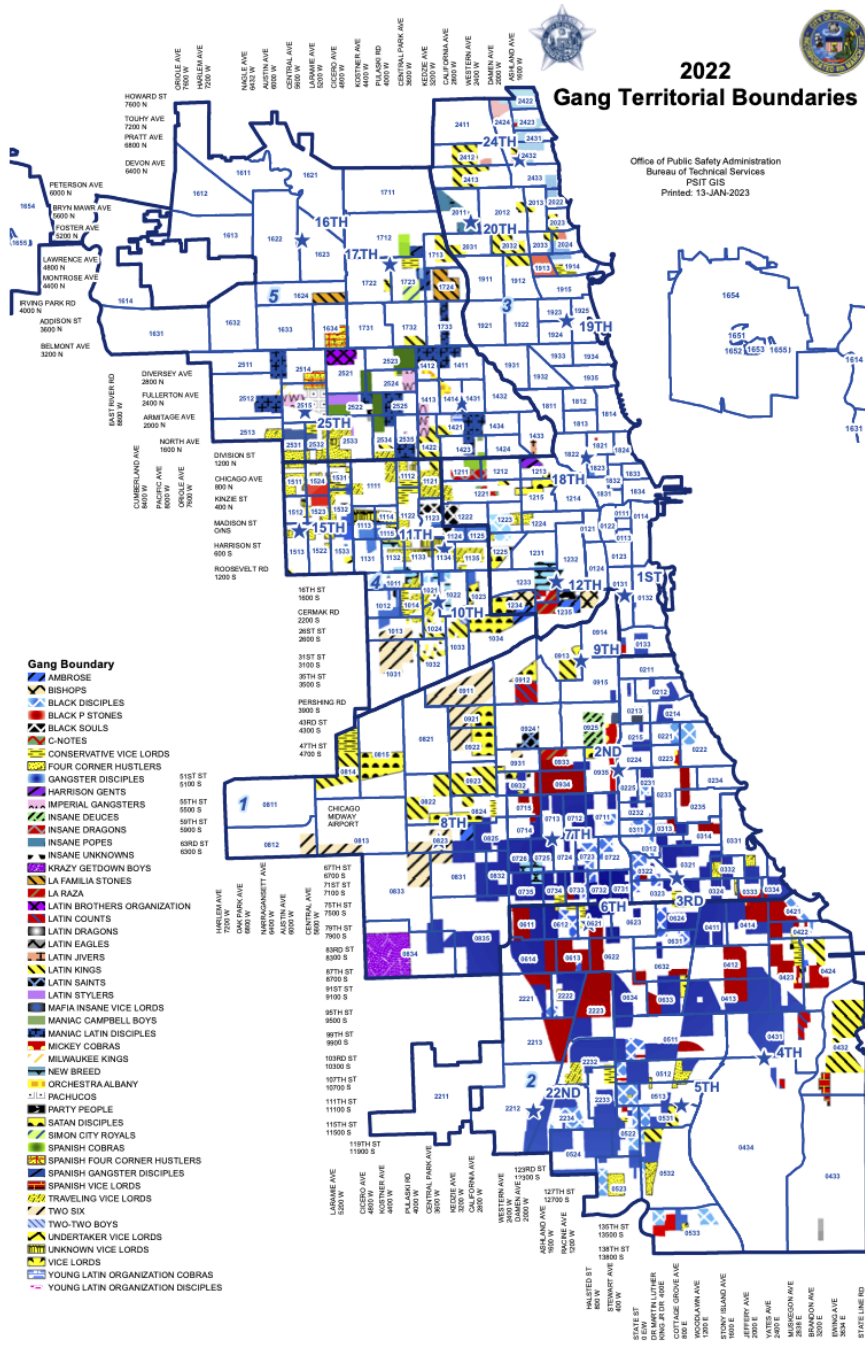


Figure 14: Full map of Chicago's gang territories in 2022 published by Chicago Police Department